

Electrochemical Performance of Dispersed Pt-M (M =V, Cr and Co) Nanoparticles for the Oxygen Reduction Electrocatalysis

Fabio H. B. Lima, M. Janete Giz and Edson A. Ticianelli*

Instituto de Química de São Carlos, Universidade de São Paulo, CP 780, 13560-970 São Carlos-SP, Brazil

A cinética da reação de redução de oxigênio (RRO) foi estudada em eletrólito de KOH em eletrodos de camada ultra fina, formados por eletrocatalisadores de Pt-V, Pt-Cr e Pt-Co dispersos em pó de carbono (Pt-M/C). As características eletrônicas e estruturais dos eletrocatalisadores foram estudadas por XANES (X-ray Absorption Near Edge Structure) e EXAFS (Extended X-ray Absorption Fine Structure) *in situ*. Voltametria cíclica e curvas de polarização do estado estacionário para a RRO foram obtidas usando a técnica de disco/anel rotatório. Os resultados de XANES para as ligas no estado oxidado mostraram um aumento na ocupação da banda 5d da Platina, enquanto que os resultados de EXAFS mostraram uma pequena redução na distância interatômica Pt-Pt em relação à Pt/C. As medidas eletroquímicas indicaram que o mecanismo via 4 elétrons é principalmente seguido para a RRO nas ligas de platina. A maior atividade eletrocatalítica foi atingida pela liga Pt-V/C, depois de tratamento térmico a 850 °C em atmosfera de hidrogênio.

The kinetics of the oxygen reduction reaction (ORR) was studied in KOH electrolyte on ultra thin layer electrodes formed by Pt-V, Pt-Cr and Pt-Co electrocatalysts dispersed on a carbon powder (Pt-M/C). The electronic and structural features of the materials were studied by *in situ* XANES (X-ray Absorption Near Edge Structure) and EXAFS (Extended X-ray Absorption Fine Structure). Cyclic voltammograms and steady state polarization curves for the ORR were obtained using the rotating ring/disk electrode technique. The XANES results for the composites in the oxidized state have shown an increase of the occupancy of the Pt 5d band while the EXAFS analyses showed some reduction of the Pt-Pt interatomic distance in the different metal alloys compared to Pt/C. The electrochemical measurements indicated that the 4-electrons mechanism is mainly followed for the ORR in these platinum alloys. The highest electrocatalytic activity was shown by the Pt-V/C alloy, after treated at 850 °C under hydrogen atmosphere.

Keywords: oxygen reduction, platinum alloys, X-ray absorption

Introduction

Several studies have been carried out in the last years aiming to increase the platinum electrocatalytic performance for the oxygen reduction reaction (ORR).¹⁻³ Some authors have reported that on Pt alloys, Pt-V, Pt-Co, Pt-Cr, Pt-Fe, etc, there is an increase of the kinetics of the ORR electrocatalysis compared to pure Pt, and this fact has been attributed to changes in the Pt-Pt bond distance, number of Pt nearest neighbors, electronic density of states of the Pt 5d band, and nature and coverage of surface oxide layers.

Toda *et al.*⁴ explained the improvement of catalytic activity based on the increases by the Pt 5d band vacancy, leading to a stronger Pt-O₂⁻ interaction. This causes

weakening and lengthening of the O-O bond and its easier scission, resulting in an increase of the reaction rate. Arico *et al.*⁵ and Shukla *et al.*⁶ have attributed the increase of the catalytic activity to a decrease of the coverage of surface oxides and an enrichment of active Pt sites. Mukerjee *et al.*⁷ have explained the enhancement of the activity based on the decrease of the Pt-Pt distance and the Pt-Pt coordination numbers. In contrast to Toda *et al.*⁴, Min. *et al.*⁸ have proposed that the oxygen reduction activity increases with the occupancy of the Pt 5d band, because it causes a decrease of the adsorption strength of oxygenated species resulting in a raise of the kinetics of the reduction of reaction intermediates.

It has been also reported⁸ that for Pt-based catalysts in acid media, as the surface area decreases (particle size increases) the specific activity for the ORR generally increases. This indicates that the oxygen reduction on the

* e-mail: edsont@iqsc.usp.br

platinum surface is a structure-sensitive reaction. The observed effect can be explained in terms of the variation of the different Pt crystal facets exposed to the electrolyte.⁹ The experiments have shown that as the surface area decreases, the exposure of Pt (100) plane grows gradually, improving the catalytic activity for the oxygen reduction reaction.

Furthermore, it has been demonstrated^{8,10} that the d-band vacancy depends on the size of the Pt particles, because the hybridization of the 5d electronic states with empty states above the Fermi level reduces the true d-electron number, and this hybridization becomes less favorable with the increase of the particle size. As mentioned above, this suggests that the adsorption strength of adsorbed oxygen species decreases, and so, the reduction of intermediates containing oxygen on the Pt surface is facilitated. However, the catalytic activity varies even with the same surface area, depending on the nature of the metal used in the alloying process, indicating that there are other factors affecting the catalytic activity in addition to the particle size.

In this paper, the electrocatalytic characteristics of the ORR on commercial platinum alloys, Pt-V/C, Pt-Cr/C and Pt-Co/C, were investigated in alkaline media. The electronic and structural features obtained by X-ray absorption spectroscopy (XAS) for these materials were used for understanding the catalytic activities, and trying to establish some structural-electronic/ORR kinetics relationships.

Experimental

Catalysts were composed by Pt-M composites, where M = V, Cr and Co (1:1 nominal atomic ratios and 20 wt.% metal/C) dispersed on carbon (from E-Tek Inc). The Pt-V/C and Pt-Cr/C materials were submitted to heat treatments under H₂ atmosphere at 500 and 850 °C for 1 h. The working electrodes were composed by the metal/C catalysts deposited as a thin layer over a pyrolytic graphite disk, 5 mm diameter (0.196 cm²), of a rotating ring/disk electrode. The ultra thin layers were prepared starting from an aqueous suspension of 2.0 mg mL⁻¹ of the metal/C produced by ultrasonically dispersing in pure water (Millipore).^{11,12} A 20 μL aliquot of the dispersed suspension was dropped on the top of the pyrolytic graphite substrate surface. After the evaporation of water, in a low vacuum condition, 20 μL of a diluted Nafion (5%, Aldrich) were dropped on the electrode surface in order to attach the catalytic particles on the pyrolytic graphite RRDE electrode substrate, and after that, dried under vacuum. Right after preparation, the electrodes were immersed into an airless 1.0 mol L⁻¹ KOH electrolyte.

A large area platinum screen served as the counter electrode and an Hg/HgO (KOH 1.0 mol L⁻¹) system was used as the reference electrode. All the experiments were carried out in 1.0 mol L⁻¹ KOH, prepared from high purity reagents (Merck) and water purified in a Milli-Q (Millipore) system.

Owing to slight contamination of the catalysts by the solvents of the Nafion solution, the electrode potentials were cycled several times between -0.88 and 0.3 V vs. Hg/HgO in order to produce a clean catalyst surface. Steady state polarization curves for the oxygen reduction were obtained in saturated oxygen conditions at several rotation rates to evaluate the ORR kinetic parameters. In this system, the ring electrode (gold) was employed to sensor the HO₂⁻ produced in the working disk electrode. This was made measuring the magnitude of the HO₂⁻ oxidation current at a constant potential of 0.1 V vs. Hg/HgO, where the oxygen reduction currents are negligible. All experiments were conducted at room temperature (25 ± 1 °C), using an AUTOLAB (PGSTAT30) potentiostat.

The *in situ* XAS measurements were performed in the Pt L₃ absorption edge using a home-built spectroelectrochemical cell.¹³ The working electrodes consisted of pellets formed with the dispersed catalysts agglutinated with PTFE (ca. 40 wt. %) and containing 10 mg cm⁻² (metal loading). Measurements were made at several electrode potentials (referred here to Hg/HgO, KOH 1.0 mol L⁻¹). The counter electrode was a Pt screen cut in the center in order to allow the free passage of the X-ray beam. Prior to the experiments, the working electrodes were soaked in the electrolyte for at least 48 h. XAS experiments were carried out at -0.7 V, -0.1 and 0.2 V vs. Hg/HgO, after cycling the electrodes in the range defined by these potentials. Results presented here correspond to the average of at least two independent measurements.

All experiments were conducted at the XAS beam line in the National Synchrotron Light Source Laboratory (LNLS), Brazil. The data acquisition system for XAS comprised three ionization detectors (incidence I₀, transmitted I_t and reference I_r). The reference channel was employed primarily for internal calibration of the edge positions by using a pure foil of the metals. Nitrogen was used in the I₀, I_t and I_r chambers. Owing to the low critical energy of the LNLS storage ring (2.08 keV), third-order harmonic contamination of the Si (111) monochromatic beam is expected to be negligible above 5 eV.¹⁴

The computer program used for the analysis of the XAS data was the WinXAS package.¹⁵ The data analysis was done according to procedures described in detail in the literature.^{16,17} Briefly, the XANES (X-ray absorption near-edge structure) spectra were first corrected for the

background absorption by fitting the pre-edge data (from -60 to -20 eV below the edge) to a linear formula, followed by extrapolation and subtraction from the data over the energy range of interest. Next, the spectra were calibrated for the edge position using the second derivative of the inflection point at the edge jump of the data from the reference channel. Finally, the spectra were normalized, taking as reference the inflection points of one of the EXAFS (extended X-ray absorption fine structure) oscillations. The EXAFS oscillations were removed from the measured absorption coefficient by using a cubic spline background subtraction. Next, the EXAFS were converted to signal per absorbing atom dividing by the height of the absorbing edge given by the fitted spline function. Fourier transforms (k^2 weighted) of the EXAFS oscillations were obtained employing the Bessel window.

Results and Discussion

Physical properties of the Pt-M/C electrocatalysts

The electronic properties of the platinum alloys were investigated by X-ray absorption near edge structure (XANES). Figure 1 shows these results obtained at the Pt L_3 edge for the Pt/C electrocatalyst in alkaline medium at several electrode potentials. Figure 2a and 2b shows the results for the Pt composites obtained at -0.7 V and 0.2 V vs. Hg/HgO, respectively. The absorption at the Pt L_3 edge (11.564 eV) corresponds to $2 p_{3/2} - 5d$ electronic transitions and the magnitude of the absorption hump or white line located at *ca.* 5 eV is directly related to the occupancy of the $5d$ electronic states, the higher is the hump the lower is the occupancy and *vice-versa*.

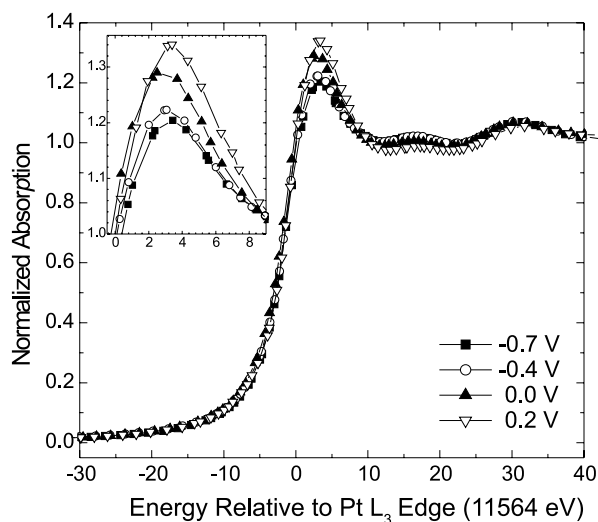


Figure 1. XANES spectra at the Pt L_3 edge for the Pt/C electrocatalysts at different electrode potentials (vs. Hg/HgO) in KOH 1.0 mol L^{-1} .

In Figure 1 it is seen that the white line magnitude increases with the increase of the electrode potential for the Pt/C catalyst in alkaline medium. This phenomenon is attributed to the emptying of the Pt $5d$ band, in agreement with the presence of an electron withdrawing effect of the oxygen present in a well-known surface oxide layer formed above -0.1 V on the catalyst particle surface.^{8,18} From Figure 2a it is seen that at -0.7 V the magnitude of the white lines is essentially the same for the different metal alloys. On the other hand, an important aspect is observed in Figure 2b, where it is seen that the increase of the Pt $5d$ band vacancy, caused by the oxide formation on Pt, is less pronounced for the alloys. These results indicate smaller Pt-oxide formation in the alloys, following a consistent trend with respect to the electronegativity of the hosting element ($V < Cr < Co$). These results are in agreement to previous XANES studies on Pt alloys in acid media.¹⁸

The XANES results obtained at -0.7 V for the Pt-V/C and Pt-Cr/C materials were heat treated in hydrogen atmosphere are presented in Figure 3a and 3b, respectively. In both cases, an increase of the Pt $5d$ band occupancy with the increase of heating temperature is observed. This effect may be caused by an increase of the catalyst particle size promoted by the heating treatment. The observed phenomena are in agreement with previous studies, which

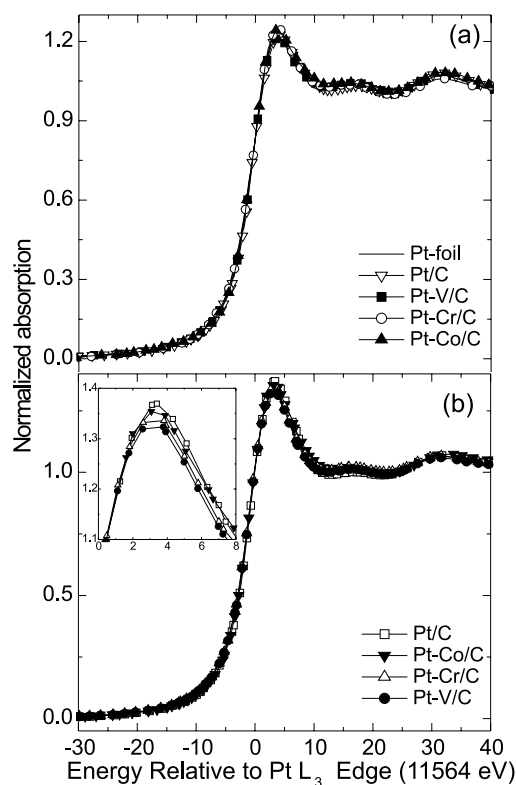


Figure 2. XANES spectra at the Pt L_3 edge for the Pt/C, for as received Pt-M/C electrocatalysts and for a Pt-foil in KOH 1.0 mol L^{-1} : (a) -0.7 V and (b) 0.2 V vs. Hg/HgO.

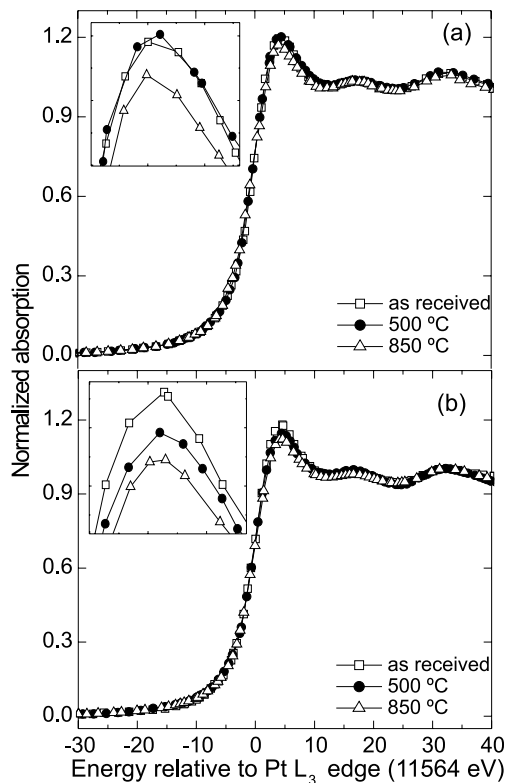


Figure 3. XANES spectra at the Pt L_3 edge on thermally treated electrocatalysts in KOH 1.0 mol L^{-1} at $-0.7 \text{ V vs. Hg/HgO}$: (a) Pt-V/C and (b) Pt-Cr/C.

showed that the d-band vacancy depends on the size of the Pt particles, because the hybridization of the 5d state with empty states above the Fermi level reduces the true d-electron number, and this is less favorable for large particles.^{8,10} Another possibility to explain the increase of the Pt 5d band occupancy may be related to an increase of the insertion of V or Cr into the Pt lattice caused by the heat treatment.

The normalized EXAFS signals obtained for a Pt foil and for the Pt/C and Pt-V/C catalysts are presented in Figure 4. The EXAFS function for the several catalysts present a great similarity with that for the Pt foil, evidencing that all materials have the same unit cell structure as pure Pt (face cubic centered, fcc). However, the EXAFS signal represents the superimposition of contributions of several coordination shells and, thus, the Fourier Transform (FT) technique is used to obtain information about the contributions of the individual shells. Peaks in the radial structure of the FT magnitude correspond to the contribution of individual coordination shells around the metallic atom under investigation.¹⁷ In Figure 5 are the FT results for the EXAFS oscillations obtained for the platinum alloys. For comparison the results for the Pt foil and for Pt/C are also included. The peak centered at *ca.* 2.6

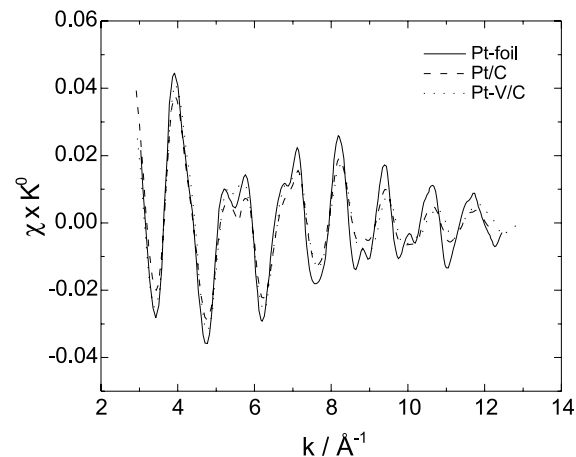


Figure 4. EXAFS signals at the Pt L_3 edge for: (solid line) Pt-foil; (dashed line) Pt/C and; (dotted line) Pt-V/C. $E = -0.7 \text{ V vs. Hg/HgO}$.

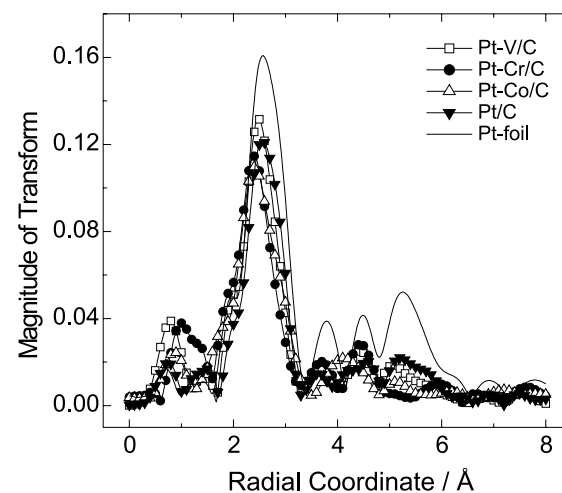


Figure 5. Fourier transform (k^3 weighted) of the EXAFS oscillations for the as received Pt-M/C electrocatalysts at $-0.7 \text{ V vs. Hg/HgO}$.

Å in the FT vs. radial coordinate plots for these materials results from the contributions related to the first Pt-Pt and Pt-M coordination shell.^{19,20} For dispersed Pt-alloys with 4d elements such as Ru and Ag, a splitting of this peak is observed^{19,20} and this is assigned to the radiation backscattering from Pt and Pt-Ru or Pt-Ag neighbors in the first shell. In Figure 5, results do not evidence a splitting of this first FT peak, in agreement with previous results for Pt-alloys with 3d elements.²¹ This is probably because the separation of both contributions is not large enough, as expect for these low atomic number Pt-coordinated backscatterers.

Further analyses of the Pt-M/C EXAFS results were made from the Pt-Pt and Pt-M first coordination shell signals in the Fourier transform. Phase and amplitude data as a function of the radial coordinate (r) were fitted to those calculated for a Pt-M/C model using the FEFF

program²² to obtain the coordination number (N), the bond distances (R), the Debye-Waller factor ($\Delta\sigma^2$), and the edge energy shift (ΔE_0). In these fittings, the limits of the radial coordinate space were chosen such that they coincide with nodes in the imaginary part of the complex Fourier transform.¹⁷ The corresponding values for Δk and Δr are summarized in Table 1. Figure 6 shows the fits in r space for the real and imaginary parts of the Fourier transform for the Pt-V/C electrocatalyst and Table 2 presents a summary of the physical parameters for all samples obtained at -0.7 V vs. Hg/HgO. For the theoretical calculations for Pt/C a S_0^2 value of 0.81 was used, and this was obtained by fitting the results for the bulk Pt foil. For the metal alloys, this parameter was iterated together with the other variables, resulting in values close to 0.7.

Table 1. Fourier transform ranges of the forward and inverse transforms (k^3 weighted) for Pt/C and Pt-M/C electrocatalysts

Electrocatalyst	$\Delta k / \text{\AA}^{-1}$	$\Delta r / \text{\AA}$
Pt/C	2.92 – 12.25	1.73 – 3.31
Pt-V/C as received	3.02 – 12.13	1.66 – 3.29
500 °C	3.03 – 12.13	1.65 – 3.27
850 °C	3.04 – 12.54	1.65 – 3.27
Pt-Cr/C	2.77 – 11.94	1.58 – 3.30
Pt-Co/C	3.25 – 11.05	1.24 – 3.36

In Table 2 it is noted a slight decrease in the Pt-Pt interatomic distance in the Pt-M/C materials, compared to Pt/C, while the Pt-M bond distances are even smaller, particularly when $M = \text{Cr}$ and Co . This indicates shrinkage of the Pt crystalline structure, this being one of the effects of the incorporation of a second metal atom with smaller radii in the Pt fcc crystals. The ratio of $N_{\text{Pt-M}} / N_{\text{Pt-Pt}}$ indicates real compositions of *ca.* 1:0.15, 1:0.9 and 1:0.6 (Pt:M) for the as received Pt-V/C, Pt-Cr/C and Pt-Co/C materials, respectively. In the case of Pt-V/C (and at lower extent for Pt-Co/C) it is seen that only a fraction of the non-noble metal atoms is alloyed with Pt, while the other atoms must

Table 2. Results of *in situ* EXAFS analyses for the carbon supported Pt-M/C electrocatalysts at -0.7 V vs. Hg/HgO

Electrocatalyst	Coordination Shell	N	$R / \text{\AA}$	$\Delta\sigma^2 / \text{\AA}^2$	$\Delta E_0 / \text{eV}$
Pt-foil	Pt-Pt	12	2.76	0.0043	9.15
Pt/C	Pt-Pt	10.1	2.74	0.0057	7.93
Pt-V/C as received	Pt-Pt	9.5	2.72	0.0053	6.55
	Pt-V	1.4	2.69	0.0057	6.55
500°C	Pt-Pt	9.3	2.72	0.0040	6.64
	Pt-V	1.6	2.70	0.0066	6.64
850°C	Pt-Pt	8.8	2.72	0.0051	8.07
	Pt-V	1.9	2.69	0.0036	8.07
Pt-Cr/C	Pt-Pt	6.3	2.70	0.0037	0.84
	Pt-Cr	5.7	2.63	0.0030	0.84
Pt-Co/C	Pt-Pt	7.0	2.71	0.0026	5.63
	Pt-Co	4.1	2.62	0.0162	5.63

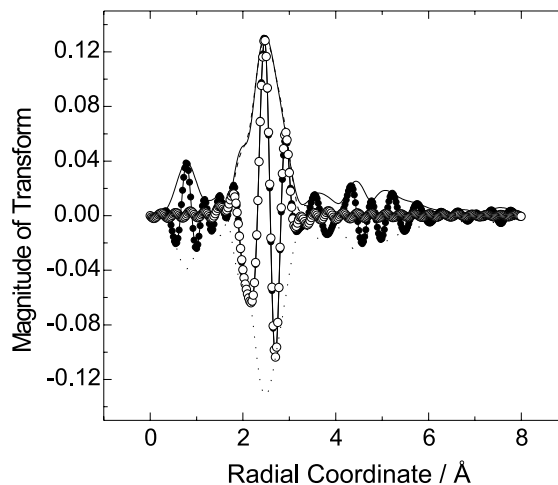


Figure 6. A first-shell fit of Pt EXAFS (k^3 weighted) for Pt-V/C in r space: (solid line) experimental FT; (dotted line) experimental FT phase; fit of (●) FT amplitude and (○) phase.

be forming an amorphous oxide phase, as already proposed based on XRD (X-ray diffraction) results.^{2,3} The small incorporation of the V atoms explains the little effect on the Pt-Pt bond distance observed for this material (Table 2). The heating treatment leads to some incorporation of V atoms in the Pt lattice, but the final proportion does not exceed 1:0.2 (Pt:V).

Electrochemical characteristics

Cyclic voltammetric profiles are shown in Figure 7 for the different Pt alloys. The results show the typical behavior regarding the hydrogen and the oxide regions of Pt/C and Pt alloys in alkaline solutions.²³ The comparison of the results (Figure 7a) evidences a small shift to anodic directions of the platinum oxide reduction peak positions for Pt-V/C and Pt-Cr/C, compared to Pt/C. In the case of Pt-Co/C, this phenomenon could not be observed, because of the presence of a redox pair located at around $-0.2 / -0.5$ V, assigned to an oxi-reduction process involving

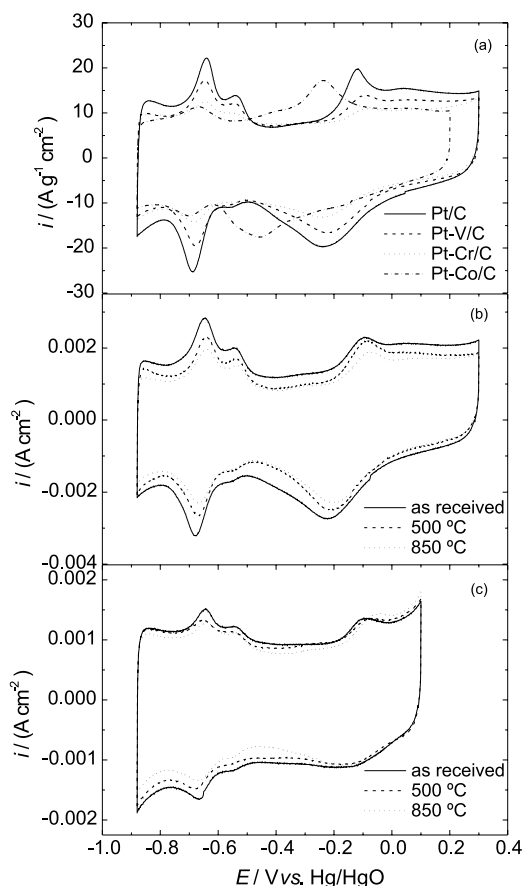


Figure 7. Cyclic voltammograms obtained for the Pt alloys in 1.0 mol L⁻¹ KOH at 0.1 V s⁻¹. (a) Comparison of the response of the different Pt alloys, (b) Pt-V/C thermally treated and (c) Pt-Cr/C thermally treated.

metallic Co.³ Anodic shifts on the reduction peak can be attributed to a decrease of the desorption free energy (ΔG_{ads}) of Pt-OH, Pt-O or Pt-O₂, due to the presence of the alloying element. This means that the adsorption strength of adsorbed oxygen species on Pt in the alloy is lower than on Pt/C and so, the reduction of intermediates containing oxygen is more facile. This fact may be associated to the higher occupancy of the Pt 5d band for the alloys in the oxidized state, compared to Pt/C, as evidenced by the results in Figure 2b.

Steady state polarization curves for the ORR and the currents for the HO₂⁻ oxidation in the ring obtained at several rotation speeds for the Pt-V/C catalyst treated at 850 °C are shown in Figure 8. The expected increase in the limiting diffusion current density in the disk (Figure 8b) is observed as a function of the rotation speed.³ On the other hand, the ring response (Figure 8a) clearly denotes formation of HO₂⁻ as an intermediate of the ORR. Figure 9 compares the ring/disk results at 1600 rpm for the different electrocatalysts. It is noted that the ORR limiting current densities assume close values for all Pt alloys, all showing

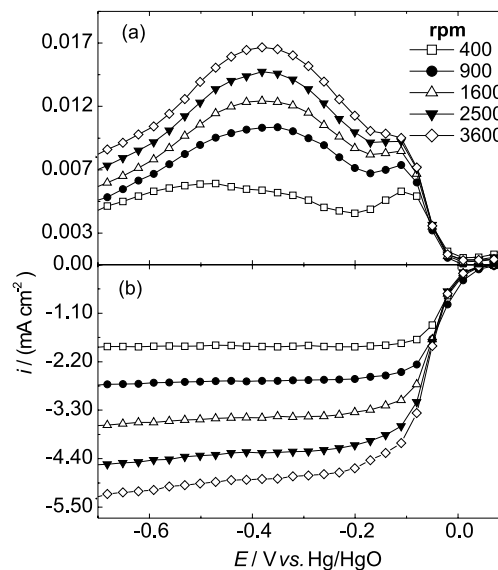


Figure 8. Rotating ring/disk results for the ORR in KOH 1.0 mol L⁻¹ at 25 °C at several rotation speeds for the Pt-V/C electrocatalyst; (a) ring currents and (b) disk currents.

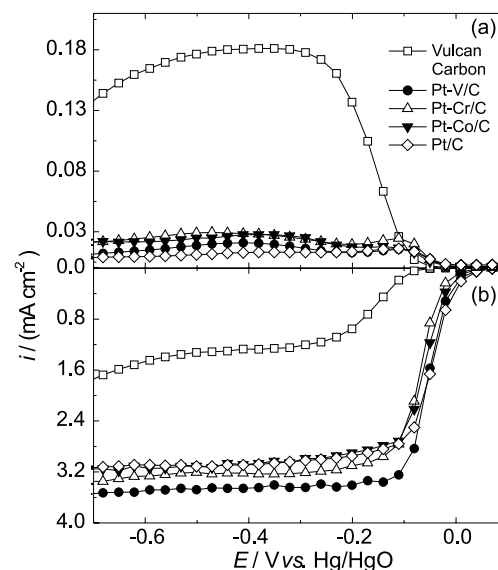


Figure 9. Rotating ring/disk results for the ORR in the Pt/C and the as received Pt-M/C catalysts in KOH 1.0 mol L⁻¹ at 25 °C and 1600 rpm: (a) ring currents and (b) disk currents.

low ring current signals for peroxide oxidation. However, the polarization curve for the Vulcan carbon shows lower limiting current for the ORR and much higher ring current signals. Since on Vulcan carbon the ORR takes place following the 2-electron mechanism,²³ forming large amounts of HO₂⁻ (see below), the small ring signals appearing for the platinum alloy electrocatalysts indicate small formation of HO₂⁻. Figure 10 shows the ring/disk results for heat-treated Pt-Cr/C in hydrogen atmosphere at 500 and 850 °C. Although the currents for HO₂⁻ oxidation are ten times smaller than for Vulcan (Figure 9), an increase

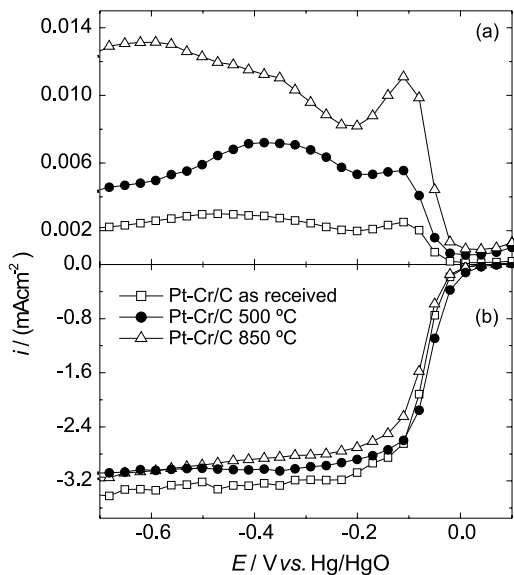


Figure 10. Rotating ring/disk results for the ORR in the Pt-Cr/C catalysts in KOH 1.0 mol L⁻¹ at 25 °C and 1600 rpm: (a) ring currents and (b) disk currents.

of formation of HO₂⁻ is noted for the materials after the thermal treatments. This is consistent with the small decrease of the limiting current density in the disk. Similar results were obtained for Pt-V/C.

The disk polarization data at several rotation speeds for each catalyst were used to construct Levich curves, as shown in Figure 11. It is seen that, except for the higher rotation rates, the Levich plots are straight lines, indicating that the oxygen diffusion is the rate-controlling step of the ORR. The linearity is not followed at high rotation speeds probably because the diffusion process becomes faster and a mixed kinetic control between the oxygen diffusion and adsorption steps is established. Values of the number of electrons (*n*) were calculated from the slope of

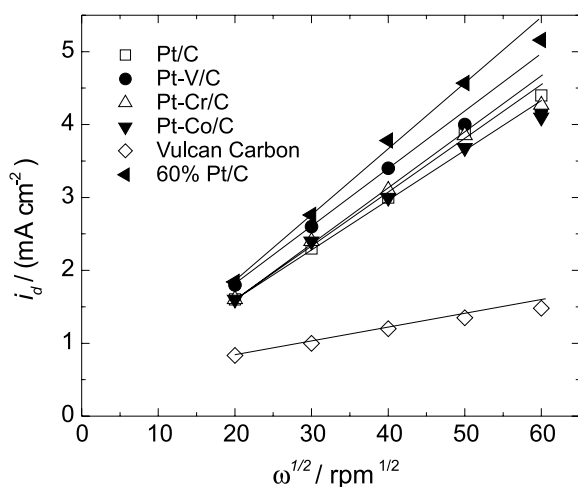


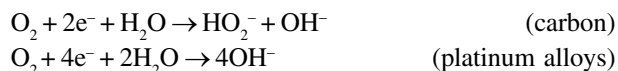
Figure 11. Levich plots for the ORR in the catalysts and for the Vulcan carbon in KOH 1.0 mol L⁻¹ at 25 °C.

the Levich lines in the linear region for all catalysts using the equation,

$$i_d = 0.620nFAD_0^{2/3}\omega^{1/2}\nu^{-1/6}C_0^* \quad (1)$$

where *i_d* is the limiting diffusion current density, *F* = Faraday constant; *D₀* = oxygen diffusion coefficient; *ω* = rotation rate in rpm; *ν* = cinematic viscosity of the solution and *C₀^{*}* = oxygen solubility in the electrolyte. These calculations were made taking the Levich line for the 60% Pt/C catalyst in the same medium as reference, and assuming *n* = 4 in this case.²³ In Figure 11 it is seen that the intercepts (*ω*^{1/2} → 0) of the Levich lines are not exactly zero as predicted by equation (1). This must be due to the current contributions not included for the derivation of equation (1), or represent a deviation of the behavior predicted by this equation due to the presence of some turbulence in the electrode/electrolyte interface caused by the high roughness of the catalyst layer.

The numbers of electrons calculated by the Levich plots are presented in Table 3. Results indicate that the ORR on the platinum alloys follows mainly a 4-electrons mechanism, also evidenced by the lower ring current signal for this electrocatalysts in relation to that for Vulcan carbon. In summary, these results are in agreement with two routes for the ORR: via two electrons (peroxide pathway) on carbon and four electrons on those platinum based catalysts:²³



The electrocatalytic activity for the ORR on the Pt alloys was compared through mass-transport corrected Tafel plots, obtained with the currents normalized by the mass of platinum in the catalyst layer. These results are shown in Figure 12. Two different Tafel linear regions were observed with slopes near 50–60 and 120 mV/dec for low

Table 3. Kinetic parameters for the ORR in the several electrocatalysts obtained from Levich and mass-transport corrected Tafel plots, in KOH 1.0 mol L⁻¹ at 25 °C

Electrocatalyst	b (V / dec)	n	<i>i_{E=0.0 V}</i> (A/g _{Pt} ⁻¹ cm ⁻²)
Vulcan Carbon	0.040	2.0	0.008
Pt/C	0.055	3.7	8.5
Pt-V/C as received	0.053	4.0	8.6
500°C	0.049	4.0	8.9
850°C	0.049	4.0	10.9
Pt-Cr/C as received	0.045	3.7	2.7
500°C	0.045	3.5	2.7
850°C	0.051	3.5	6.2
Pt-Co/C	0.046	3.5	6.2
60% Pt/C	0.060	4.0	6.2

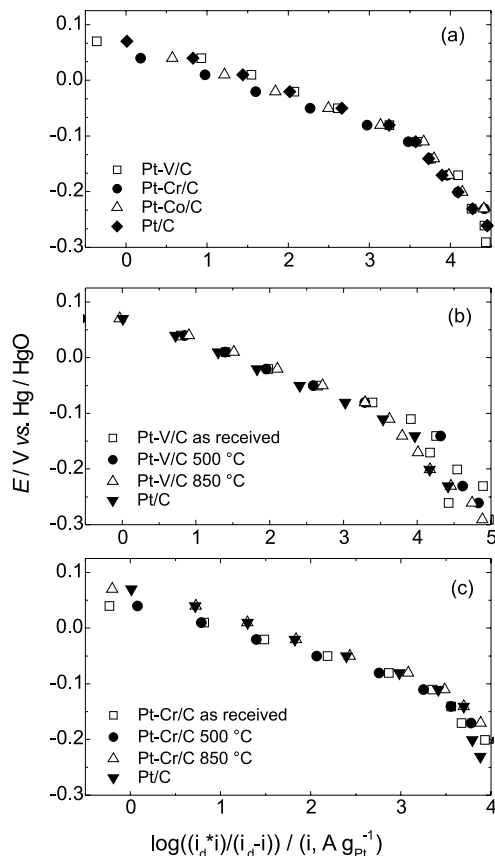


Figure 12. Mass-transport corrected Tafel plots for the ORR in the several catalysts in KOH 1.0 mol L⁻¹ at 25 °C. $\omega = 1600$ rpm. (a) Comparison of the response of the different Pt-M/C alloys, (b) Pt-V/C thermally treated and (c) Pt-Cr/C thermally treated. Currents were normalized per mass of platinum in the catalyst layer.

and high overpotentials, respectively, in agreement to previous works.²³ This can be explained in terms of the coverage of adsorbed oxygen, which follows a Temkin isotherm (high coverage) at low overpotentials and a Langmuir isotherm (low coverage) at higher overpotentials. The comparison of the catalytic activity for the several electrodes was also made from the values of the mass activity (disk current per unit Pt mass), measured at $E = 0.0$ V vs. Hg/HgO ($i_{E=0.0V}$), included in Table 3.

The results presented in Figure 12a evidence higher catalytic activity for the Pt-V/C alloy, among all the as received catalysts. The heat-treated Pt-V/C and Pt-Cr/C alloys have shown improvements in the activity with the increase in the heat treatment temperature. As seen in Table 3, the highest catalytic activity was seen for the Pt-V/C heated treated at 850 °C.

Changes in the catalytic activity observed for the different Pt-alloys can be discussed in terms of the Pt-Pt bond distance, the density of states of the Pt 5d band, and the degree of coverage of oxide surface layers on Pt. According to the EXAFS results for the platinum alloys, a

reduction of the Pt-Pt interatomic distance is observed due to the presence of the non-noble metal into the Pt fcc structure compared to pure Pt. The electrochemical ORR results have indicated that only Pt-V/C presents higher activity than Pt/C. Also, the thermal treatment did not change the interatomic distances, but a clear increase of the catalytic activity was evidenced. Thus, these results did not evidence any direct correlation of the catalytic activity with the Pt-Pt bond distance.

On the other hand, XANES results in Figure 2 clearly indicated an increase of the Pt 5d band occupancy for the oxidized Pt-alloys, compared to pure Pt. It has been claimed that an increase of the electronic occupancy of the Pt 5d band improves the ORR kinetics, because the adsorption strength of oxygen species decreases, and so, the reduction of adsorbed oxygen intermediate becomes more facile. On the basis of these facts one would expect that all the three alloys should present higher activity compared to Pt/C, but this trend was not confirmed for Pt-Cr/C and Pt-Co/C.

As observed before, pure vanadium, cobalt or chromium are very little active for the oxygen reduction reaction in alkaline solutions.²⁴ So, the presence of such atoms in the surface of the alloy particles (possible as oxides) could have a screening effect on neighboring Pt atoms lowering the number of active sites for the oxygen reduction reaction.²⁵ Thus, the higher is the M:Pt proportion, the higher would be the screening effect. Here, in the cases of Pt-Cr/C and Pt-Co/C, which present large M:Pt proportion (more close to 1:1, according the N_{Pt-M} / N_{Pt-Pt} in Table 2), the screening effect may predominate over the beneficial effect on the Pt 5d band, resulting in a lower oxygen reduction activity compared to Pt/C (Figure 12 and Table 3). In the case of Pt-V/C, the small V:M proportion may result in the predominance of the electronic effects over the screening effect, leading to higher ORR kinetics.

Conclusions

The XANES measurements for the different metal alloys indicated a reduction of the Pt 5d band vacancy in the oxide region due to the presence of the non-noble metal, the highest effect being for Pt-V/C. Increasing the heat treatment temperature resulted in an increase of the Pt 5d band occupancy for both Pt-V/C and Pt-Cr/C. The EXAFS analyses have shown some shrinkage in the Pt-Pt interatomic distances for the platinum alloys, with negligible effect of the heat treatment.

Polarization results have indicated a higher catalytic activity for Pt-V/C material and evidenced an increase of the activity with the increase of heat treatment temperature.

This was attributed to a lowering of the adsorption strength of adsorbed oxygen species caused by the increase of the Pt 5d occupancy promoted by the V atoms in the Pt lattice.

Acknowledgments

The authors thank the Fundação de Amparo à Pesquisa do Estado de São Paulo (FAPESP), the Conselho Nacional de Desenvolvimento Científico e Tecnológico (CNPq), and the National Synchrotron Light Source Laboratory (LNLS), Brazil, for financial assistance.

References

1. Xiong, L.; Kannan, A.M.; Manthiram, A.; *Electrochem. Comm.* **2002**, *4*, 898.
2. Antolini, E.; Passos R. R.; Ticianelli, E.A.; *Electrochim. Acta* **2002**, *48*, 263.
3. Lima, F.H.B.; Ticianelli E.A.; *Electrochim. Acta* **2004**, *49*, 4091.
4. Toda, T.; Igarashi, H.; Watanabe, M.; *J. Electroanal. Chem.* **1999**, *460*, 258.
5. Arico, A.S.; Shukla, A.K.; Kim, H.; Park, S.; Min, M.; Antonucci, V.; *Appl. Surf. Sci.* **2001**, *172*, 33.
6. Shukla, A.K.; Neergat M.; Bera, P.; Jayaram V.; Hegde, M.S.; *J. Electroanal. Chem* **2001**, *504*, 111.
7. Mukerjee, S.; Srinivasan, S.; Soriaga, M.P.; McBreen, J.; *J. Phys. Chem.* **1995**, *99*, 4577.
8. Min, M.; Cho, J.; Cho, K.; Kim, H.; *Electrochim. Acta* **2000**, *45*, 4211.
9. Cho, J.; Roh, W.; Kim, D.; Yoon, J.; Choy, J.; Kim, H.; *J. Electrochem. Soc. Faraday Trans.* **1998**, *94*, 2835.
10. Yoshitake, H.; Iwasawa, Y.; *J. Phys. Chem.* **1992**, *96*, 1329.
11. Gloaguen, F.; Andolfatto, F.; Durand, R.; Ozil, P.; *J. Appl. Electrochem.* **1994**, *24*, 863.
12. Schmidt, T.J.; Gasteiger, H.A.; Stäb, G.D.; Urban, P.M.; Kolb, D.M.; Behm, R.J.; *J. Electrochem. Soc.* **1998**, *145*, 2354.
13. McBreem, J.; O'Grady, W.E.; Pandya, K.I.; Roffman, R.W.; Sayers, D.E.; *Langmuir* **1987**, *3*, 428.
14. Tolentino, H.; Cezar, J.C.; Cruz, D.Z.; Compagnon-Caillol, V.; Tamura, E.; Alves M.C.; *J. Synchrotron Radiat.* **1998**, *5*, 521.
15. Ressler, T.; *J. Phys. IV* **1997**, *C2 7*, 269.
16. Pandya, K.I.; Roffman, R.W.; McBreen J.; O'Grady, W.E.; *J. Electrochem. Soc.* **1990**, *137*, 383.
17. van Zon, J.B.A.C.; Konigsberger, D.C.; Van't Blik, H.F.J., Sayers, D.E.; *J. Chem. Phys.* **1985**, *82*, 5742.
18. McBreen, J.; Mukerjee, S.; *J. Electrochem. Soc.* **1995**, *142*, 3399.
19. Câmara, G.A.; Giz, M.J.; Paganin, V.A.; Ticianelli, E.A.; *J. Electroanal. Chem.* **2002** *537*, 21.
20. Lima, F.H.B.; Sanches, C.D.; Ticianelli, E.A.; *J. Electrochem. Soc.*, in press.
21. Mukerjee, S.; Srinivasan, S.; Soriaga, M.P.; McBreen, J.; *J. Electrochem. Soc.* **1995**, *142*, 1409.
22. Rehr, J.J.; Albers, R.C.; *Phys. Rev. Sect. B* **1990**, *41*, 139.
23. Perez, J.; Gonzalez, E.R.; Ticianelli, E.A.; *Electrochim. Acta* **1998**, *44*, 1329.
24. Obradovic, M.D., Grgur, B.N., Vracar, Lj.M.; *J. Electroanal. Chem.* **2003**, *548*, 69.
25. Paulus, U.A.; Wokaum, A.; Sherer, G.G.; Schmidt, T.J.; Stamenkovic V.; Markovic N. 25. M.; Ross, P.N.; *Electrochim. Acta* **2002**, *47*, 3787.

Received: November 15, 2004

Published on the web: March 6, 2005

FAPESP helped in meeting the publication costs of this article.